A fluorescent ratiometric nanosized system for the determination of Pd^{II} in water†

Massimiliano Arca, Claudia Caltagirone, Greta De Filippo, Mauro Formica, Vieri Fusi, Luca Giorgi, Vito Lippolis, Luca Prodi, Enrico Rampazzo, Mariano Andrea Scorciapino, Massimo Sgarzi, Nelsi Zaccheroni

Electronic Supplementary Informations

Synthesis

All chemicals were purchased from Aldrich in the highest quality commercially available. All the solvents were dried prior to use. The synthetic pathway used to obtain the ligand **L** is reported in Scheme S1. The 2,8-dithia-5-aza-2,6-pyridinophane **1** was prepared as described.[1]

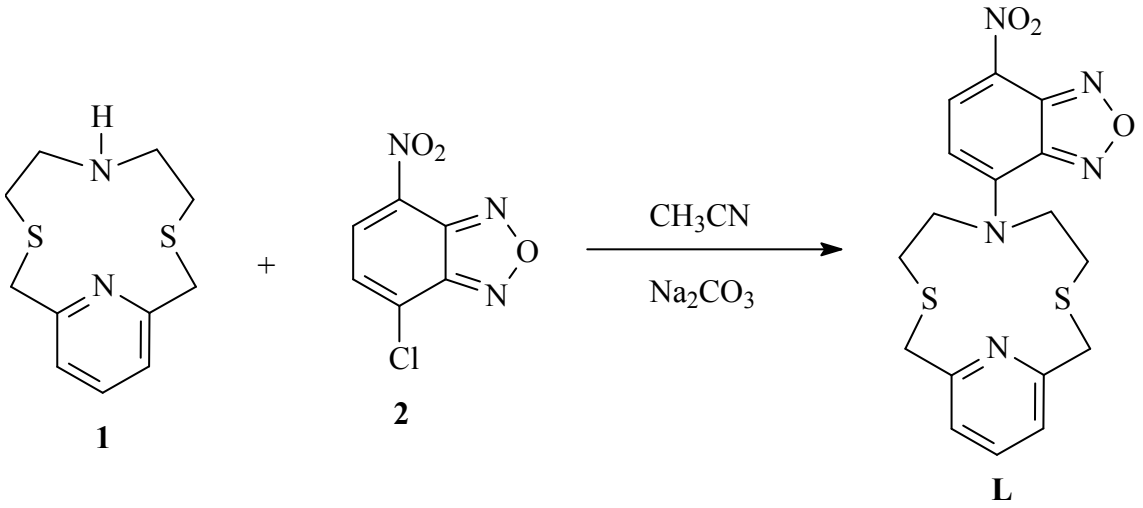

Scheme S1: Synthesis of **L**

5-(7-nitrobenzo[1,2,5]oxadiazole-4-yl)-2,8-dithia-5-aza-2,6-pyridinophane (L)

A solution of 7-nitrobenzo[1,2,5]oxadiazole-4-yl (240 mg, 1,0 mmol) in dry MeCN (20 mL) was added in an inert atmosphere and dropwise to a mixture of 2,8-dithia-5-aza-2,6-pyridinophane (220 mg, 1,1 mmol) and Na_2CO_3 (640 mg, 6 mmol) in dry MeCN (50 mL). The mixture was stirred at room temperature for 24 h. Na_2CO_3 was then filtered off and the solvent was removed under reduced pressure. The resulting crude product was washed with Et_2O to give a red-brown solid (330 mg, yield 81%). Elem Anal (%) calcd for $C_{17}H_{17}N_5O_3S_2$: C, 50.61; H, 4.25; N, 17.36; found: C,

50.3; H, 4.5; N, 17.1 ^{1}H NMR (200,13 MHz, CD_3CN, ppm): δ_H 2.76–2.68 (m, 8H, SC*H2*C*H2*N), 4.00 (s, 4H, PyC*H2*S), 6.35 (d, J=9,2 Hz, 1H, NBD), 7.44 (d, J=7,6 Hz, 2H, Py), 7.86 (t, J=7,6 Hz, 1H, Py), 7.39 (d, J=9,2 Hz, 1H, NBD). ^{13}C NMR (50,33 MHz, DMSO-*d6*, ppm): δ_C 26.8 (S*C*H_2CH_2N), 36.4 (Py*C*H_2S), 53.1 (SCH_2*C*H_2N), 103.0, 121.3, 122.7, 136.7, 139.5, 144.6, 145.2, 145.4, 157.8.

PdLCl_2

Ligand **L** (10 mg, 0,025 mmol) and potassium tetrachloropalladate (K_2PdCl_4, 9 mg, 0,028 mmol) were dissolved in dry DMF (5 mL) and stirred at 100°C overnigth. The solution was cooled at room temperature obtaining the complex as a red precipitate. The solid was filtered and washed with ethanol to remove any trace of DMF affording 11 mg of pure complex (yield 78% with respect **L**). MS-ESI: m/z=579.9 (M+H). Elem Anal (%) calcd for $C_{17}H_{17}Cl_2N_5O_3PdS_2$: C, 35.16; H, 2.95; N, 12.06; found: C, 35.3; H, 3,1; N, 12.0.

Figure S1. Relative emission intensity at 540 nm of **L** and K_2PdCl_4 in 1:1 molar ratio and in co-presence of 10 equiv. of another metal ion (perchlorate and K_2PtCl_4 salts were used) in DMF/Water 4:1 (v/v) ($2 \cdot 10^{-5}$ M, λ_{ex}=340 nm). Measurements were made soon after the mixing of the reagents and were stable in time.

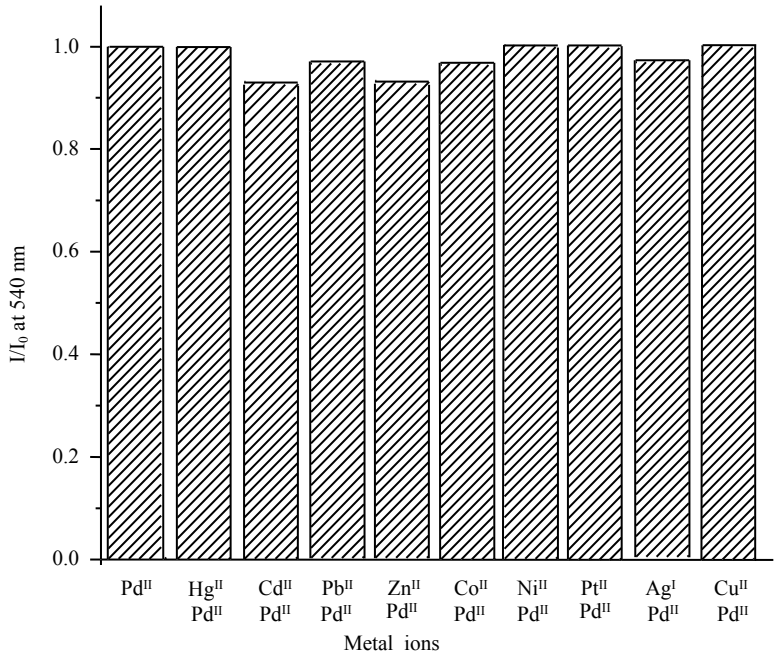

Determination of the structure of the Pd^{II}/L complex by NMR experiments

NMR analyses

Figure S2 shows the stack plot of the ^{1}H-NMR spectra acquired on **L** in DMF-d_7 titrated with increasing Pd equivalents. The latter are reported of the left side of each spectrum.

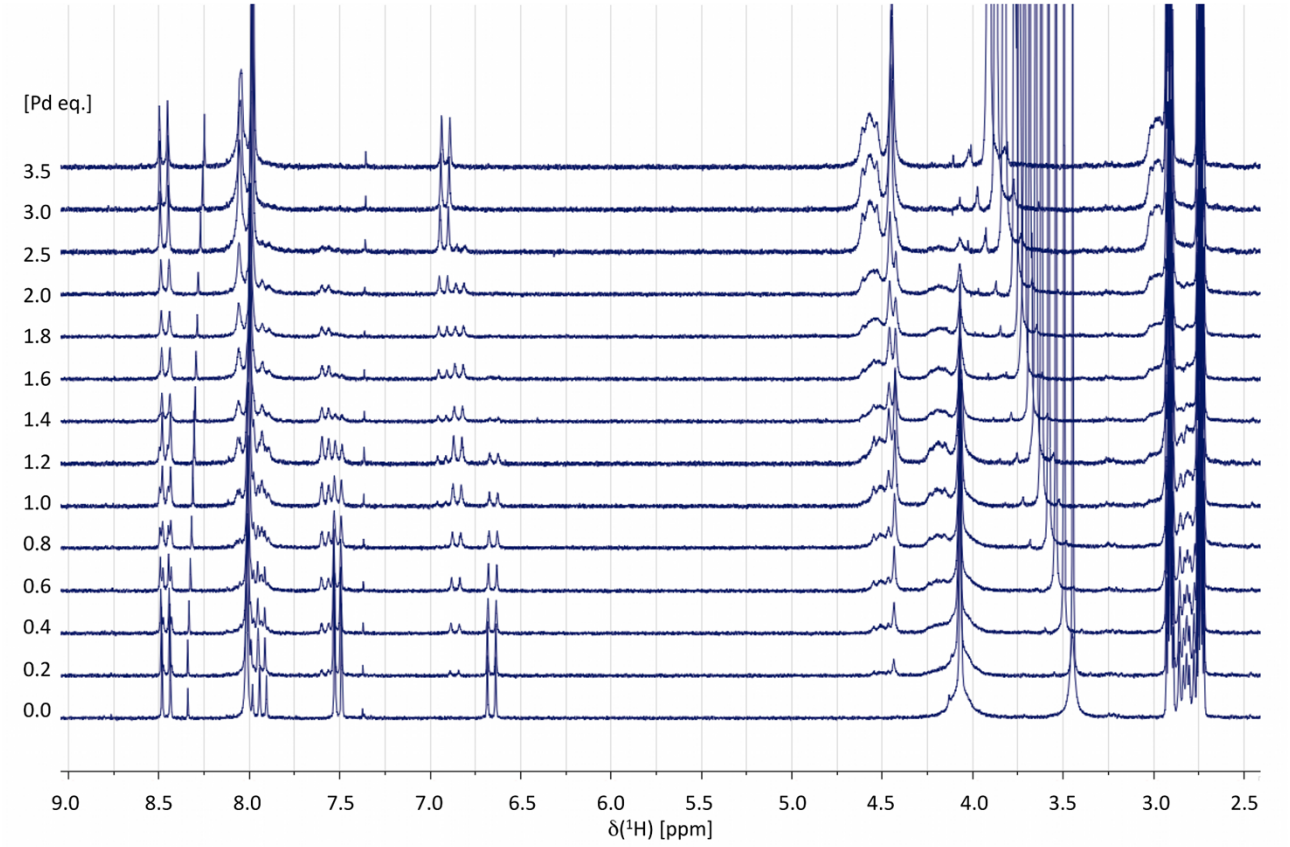

Resonance assignments were obtained by the analysis of two-dimensional homonuclear COSY and NOESY spectra, as well as by inspection of signals relative integrated areas and multiplicity, and are reported in Scheme 1 for **L** in the absence of Pd.

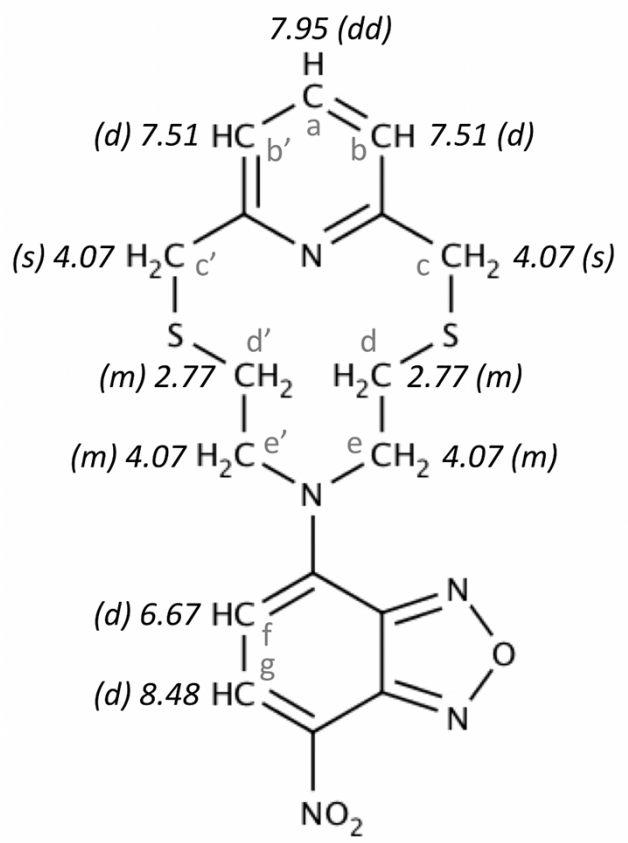

Scheme 1. Schematic molecular representation of **L**. The ^{1}H chemical shift values observed in DMF-d_7 in the absence of Pd^{II} are reported next to each protons group, which are also labeled with lowercase letters from *a* to *g* for the sake of clarity. Signals multiplicity is given in parentheses (*d* doublet; *dd* doublet of doublets; *m* 2nd order multiplet; *s* singlet).

As soon as Pd was added to the solution, new resonances were observed in the spectrum, whose relative intensity increased with increasing Pd^{II} concentration. The relative intensity of the resonances observed for **L** in the absence of Pd^{II} decreased correspondingly. Then, with further increasing the Pd^{II} equivalents, the intensity of such 'new' resonances started to decrease, while a third series of signals emerged in the spectrum.

The case of the doublet attributed to the proton *f* (Scheme 1) at 6.67 ppm (Figure S2) is particularly evident and informative. The relative intensity of this resonance decreased with increasing the Pd^{II} concentration, completely disappearing under the spectral noise at 1.8 eq. of Pd^{II}. A second doublet at 6.87 ppm started to emerge already at 0.2 eq. of Pd^{II}, with its relative intensity increasing with increasing Pd^{II} concentration. This resonance reached the maximum around 1 eq. and then started to decrease, until, in the spectra recorded in the presence of 3.0 eq. of Pd^{II}, it was no more detectable.

A third doublet was also observed at 6.96 ppm from 1 eq. up to the end of the titration performed in the present study, with a relative intensity increasing with the Pd^{II} concentration.

These data strongly suggest that three different species are in equilibrium during the titration, the first one corresponding to the free **L**, the second to a 1:1 complex, while the third one is attributable to a 2:1 Pd/**L** complex. Moreover, the observation of the resonances for all the three species together and well resolved in the same spectra indicates that the Pd exchange rate is slow with respect to the NMR time-scale, i.e. $k_{ex} << \Delta\nu$, where $\Delta\nu$ is the frequency difference between the resonances, thus, << 17 s^{-1}.[2] Figure S3 shows the distribution diagram obtained from the NMR data using the relative intensity of the three aforementioned doublets to calculate the molar fraction of the corresponding species.

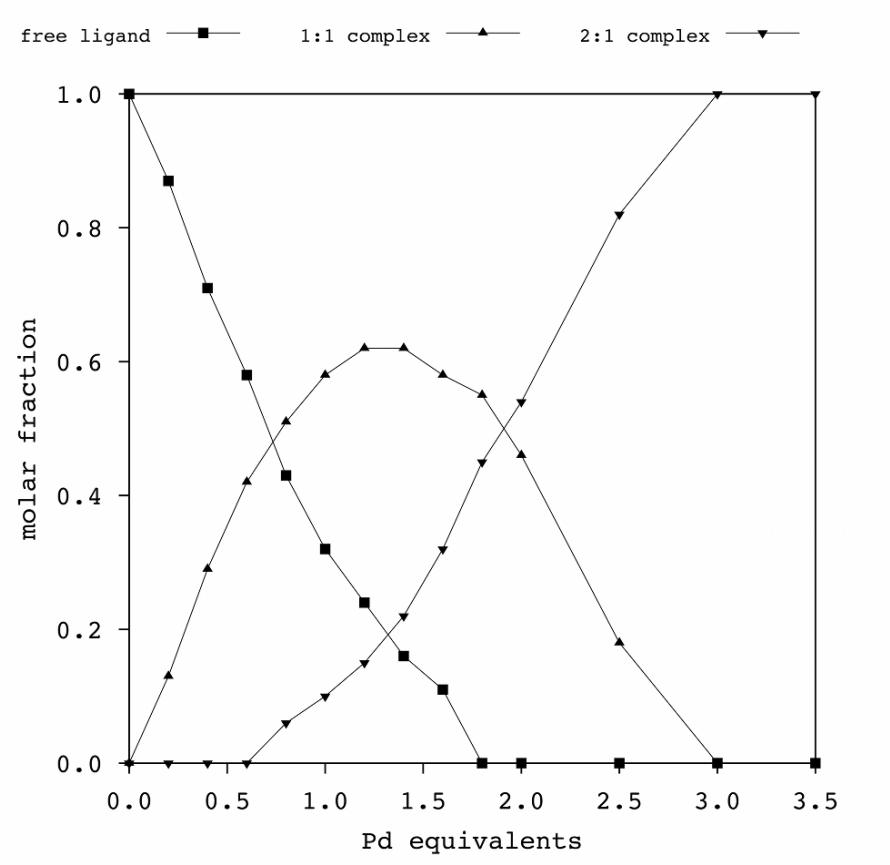

Figure S3. Distribution diagram of the free **L**, 1:1 and 2:1 Pd/**L** complexes obtained from the ^{1}H-NMR integrated resonances of proton *f* (Scheme 1) in DMF-d_7.

Accordingly, similar trends could be observed for the other resonances, although the lower separation between the signals and/or the superimposition with the solvent peaks (e.g. for the resonances *a*, *b* and *d*) did not allow for an accurate signal integration.

Nevertheless, the case of protons *c* and *e* is particularly interesting. Figure S4(A-C) shows the 3.9-4.8 ppm range for three selected ^{1}H spectra from the titration series in figure S2, namely, the spectrum acquired in the absence of Pd^{II}, and those collected in the presence of 1.2 and 2.0 equivalents. The four protons *c*, as well as all of the four protons *e*, resonated at 4.07 ppm in the absence of Pd^{II} (figure S4A), as expected due to molecular symmetry. However, as said, several resonances emerged in the presence of Pd^{II} and, at 1.2 eq., three species were in equilibrium, as shown by the distribution diagram in figure S3. The peak at 4.07 ppm is still clearly visible in the spectrum (figure S4B), but other two singlets arouse at 4.09 and 4.44 ppm, respectively, during the first half of the titration. Both these two resonances are accompanied by one multiplet each, located at a slightly higher frequency, ~ 4.2 and ~ 4.5 ppm, respectively. The trend of the relative intensity vs. Pd^{II} equivalents for these four resonances was the same as that observed for the doublet *f* at 6.87 ppm described above, thus ascribable to the formation of the 1:1 complex. Finally, a third singlet is clearly observed at 4.48 ppm, whose relative intensity vs. Pd^{II} equivalents was the same ascribed to the formation of the 2:1 complex. Indeed, with further increasing the Pd^{II} concentration (figure S4C), the relative intensity of all the aforementioned resonances decreased but the latter. Both the singlet at 4.48 ppm and its associated multiplet at 4.57 ppm became clearly visible during the second half of the titration.

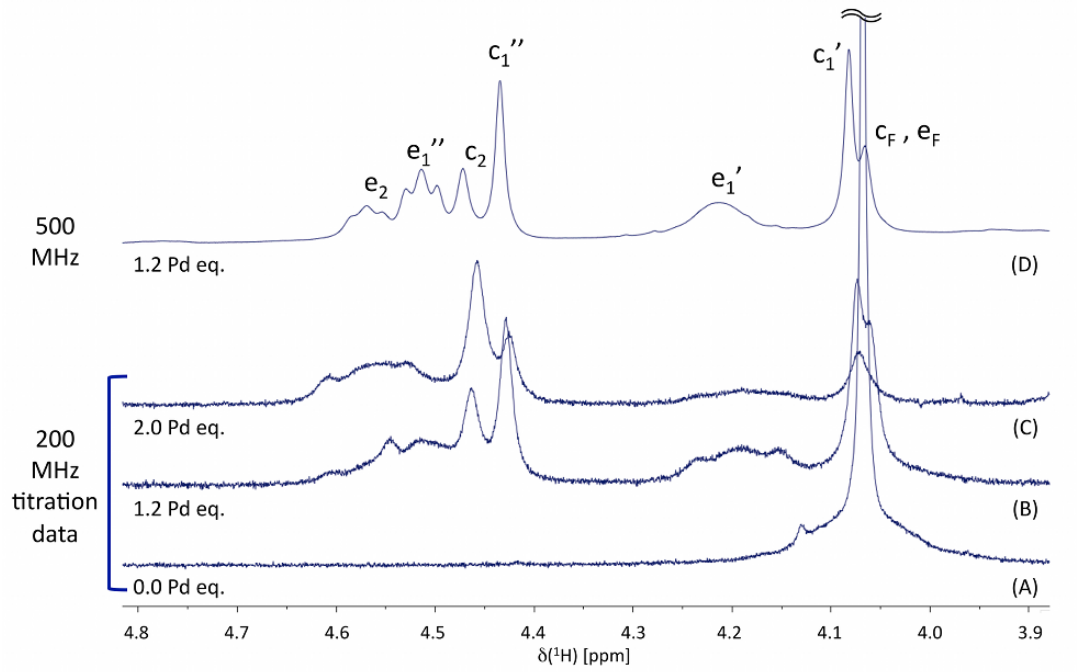

Figure S4. Stack plot of three selected ^{1}H-NMR spectra **(A-C)** from Figure S2 zoomed in the 3.9-4.8 ppm range, together with **(D)** the spectrum acquired with a 500MHz spectrometer on a sample prepared with 1.2 eq. of Pd^{II}. Differently from Fig. 2 in the main paper, resonance assignments are shown for the spectrum **(D)** using the same lowercase letters as in Scheme 1, together with a subscript to indicate the free ligand (F), the 1:1 complex (1) or the 2:1 complex (2). In the case of the 1:1 complex, also the superscript ‘ and ‘’ had to be used to label the different resonances corresponding to the chemically equivalent but magnetically inequivalent groups due to the asymmetry of the complex.

In order to achieve a better understanding of the **L**-Pd interactions, further NMR spectra were recorded with a higher magnetic field, namely, with a spectrometer operating at a proton Larmor frequency of 500 MHz, aiming at improving both signal/noise ratio and spectral resolution. The sample of choice was the one with 1.2 eq. of Pd^{II}, where all the three species were present. The ^{1}H NMR spectrum is shown in figure S4D in the same 3.9-4.8 ppm range. All of the aforementioned resonances pertaining to the different species at equilibrium resulted to be well resolved and, according to the DQF-COSY and NOESY correlations, the complete resonances assignment could be performed, as shown by the labels reported in the figure. The results showed that, in the absence of Pd^{II}, the ligand is absolutely symmetric from the NMR point of view, i.e. the four *c* as well as the four *e* protons are magnetically equivalent. On the contrary, upon formation of the 1:1 complex, Pd

interacts with the ligand in a way that both the *c* protons and the *e* protons (as well as the *d* protons, not shown) lose their equivalence. On the basis of the relative intensity of the corresponding resonances and the correlations observed in the two-dimensional spectra, two protons *c* resonated at 4.09 ppm while the other two were found at 4.44 ppm. Similarly, two protons *e* were found at 4.21 ppm, the other two at 4.51 ppm. Interestingly, symmetry was regained in the 2:1 complex, as shown by a unique resonance for all the four protons *c* as well as by a unique resonance for the four protons *e*, at 4.48 and 4.57 ppm, respectively.

A possible explanation for the asymmetry of the Pd-**L** interaction characterizing the 1:1 complex could be that the Pd is centrally located on one side of the molecule, interacting with both the two nitrogen and the two sulfur atoms. This should cause one proton for each methylenic groups *c*, *d* and *e* to be closer to the Pd than the other, thus generating a sort of "plane-asymmetry" that would explain the different chemical shift. Otherwise, Pd^{II} might interact with only one nitrogen and one sulfur at a time, generating a "lateral-asymmetry" that would equivalently explain the NMR observations, i.e. one methylen-*c*, one methylen-*d* and one methylen-*e* being closer to the Pd than their corresponding counterparts on the other side of the molecule. Unfortunately, the ^{1}H homonuclear two-dimensional experiments were unable to solve this ambiguity, since the same cross-peaks pattern is expected for both the hypotheses.

However, in the case of "plane-asymmetry", both the ^{1}H resonances labeled with c_1' and c_1'' in figure S4 should correlate with exactly the same carbon resonance in a two-dimensional heteronuclear experiments. The same should apply to the proton resonances e_1' and e_1'', as well as to the d_1' and d_1''. Conversely, in the case of a "lateral-asymmetry", homologous proton resonances should be found to correlate with a different carbon resonance, since the chemical shift of the homologous ^{13}C nuclei would be differently affected by Pd binding. This was exactly the case of the $^{1}H^{13}C$-gHSQC we acquired on the selected sample (Fig. S6), demonstrating the "lateral-symmetry" for the **L**/Pd 1:1 complex. All the resonances chemical shift values and the corresponding attribution are reported in Table S1 for both ^{1}H and ^{13}C.

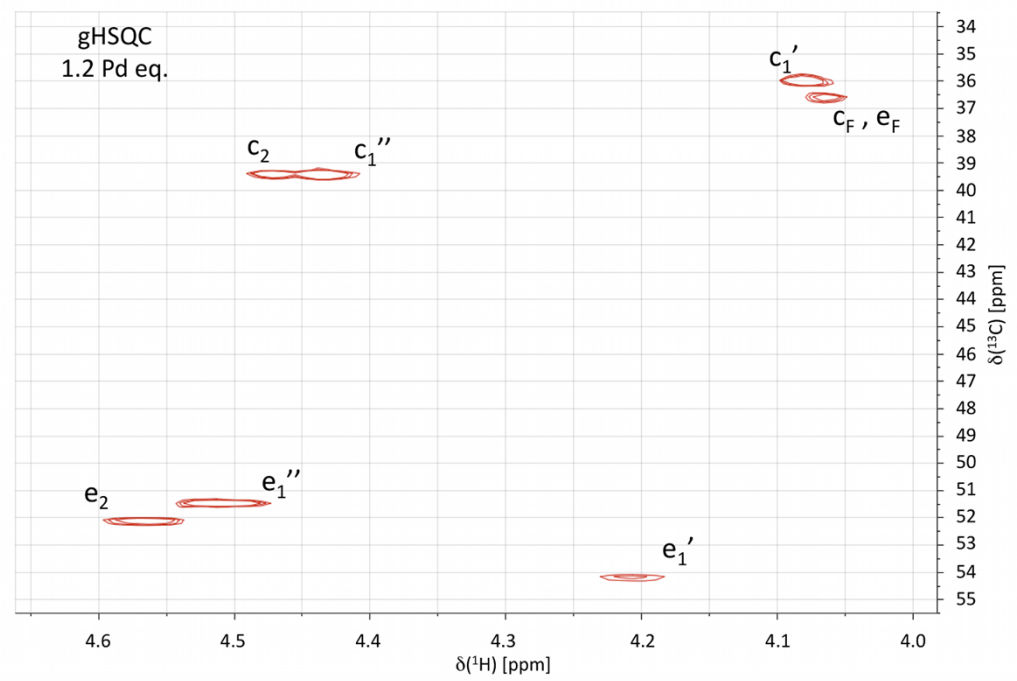

Figure S5. $^{1}H^{13}C$-gHSQC two-dimensional spectrum zoomed in the region showing correlations of the resonances of figure S4. The spectrum was acquired with a 500MHz spectrometer on the sample prepared with 1.2 eq. of Pd^{II}. Similarly to figure S4, resonance assignments are shown using the same lowercase letters as in Scheme 1, together with a subscript to indicate the free ligand (F), the 1:1 complex (1) or the 2:1 complex (2). The superscript ‘ and ‘’ had to be used in addition, in the case of the 1:1 complex, to label the different resonances corresponding to the chemically equivalent but magnetically inequivalent groups due to the asymmetry of the complex.

Table S1. ^{1}H and ^{13}C NMR resonance assignments for the free **L**, the 1:1 and 2:1 **L**/Pd complex.

^{1}H [ppm]				^{13}C [ppm]			
nuclei[a]	free	1:1	2:1	free	1:1	2:1	nuclei[a]
a	7.95	8.01	8.01	139.40	139.65	139.65	a
b	7.51	7.59	7.92	122.67	123.77	123.91	b
c	4.07	4.09 4.44	4.48	36.53	35.94 39.33	39.33	c
d	2.77	2.80 2.90	2.99	27.33	27.33 28.90	30.28	d
e	4.07	4.21 4.51	4.57	36.53	54.14 51.42	52.07	e
f	6.67	6.87	6.96	102.85	103.27	103.76	f
g	8.48	8.46	8.46	136.35	136.16	136.16	g
[a] The same labels as in figure 2 are used.							

The analysis of the homonuclear NOESY revealed several dipolar correlations between the resonances ascribed to the different proton groups of the ligand in the 1:1 complex. The relative intensity of the cross-peaks was used to restraint the corresponding inter-proton distance during a simulated annealing procedure.[3] Figure S6 shows the conformer with the lowest potential energy, according to both the experimental restraints and the force-field parameters.[4]

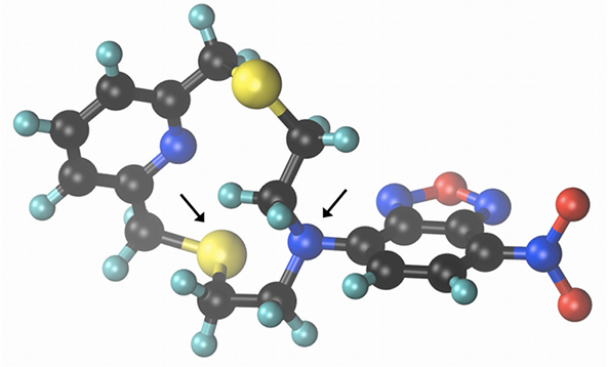

Figure S6. The lowest potential energy 3D structure obtained for **L** involved in the 1:1 complex with Pd by 1H- NMR measurements. The two arrows indicate the sulfur and nitrogen atoms likely involved in Pd^{II} coordination

Violations of the experimental NOEs have never been observed. The molecular conformation is clearly asymmetric and, taking into account the relative orientation of both the nitrogens and sulfurs lone-pairs (although these were not modeled at all in the classic approach applied here), it is plausible that Pd might be coordinated by the two atoms indicated by the arrows in Figure S6. On the other hand, the few NOEs observed for the 2:1 complex did not allowed to perform any reliable structure modeling, also in the light of resonance degeneracy for homologous chemical groups, but the NMR data showed that magnetic and (probably) conformational symmetry is regained.

NMR Experimental Methods

L was dissolved at a concentration of 16.8 mM in perdeuterated N,N-dimethylformamide (DMF). 1.2 equivalents of Pd were added as K_2PdCl_4. The samples was loaded in 5 mm test tube, and spectra were acquired with a Unity Inova 500NB high-resolution spectrometer (Agilent Technologies, CA, USA) operating at a ^1H frequency of 500 MHz, equipped with a high-field indirect detection probe. Experiments were carried out at 300 K. ^1H-NMR titration of L with Pd^{II} in DMF was performed at 200 MHz using a Bruker Avance instrument, operating at 200.13 MHz. Chemical shifts were referenced to the lower frequency methyl signal of DMF (^1H 2.746 and ^{13}C 30.13 ppm).[5] The ^1H spectrum was acquired using a 7.0 μs pulse (90°), 1 s delay time, 1.5 s acquisition time and a spectral width of 8.5 kHz. ^1H–^1H correlation DQF-COSY experiments were recorded over the same spectral window using 2048 complex points and sampling each of the 512 increments with 64 scans. The same acquisition parameters have been applied, together with a mixing time of 100 ms, for the acquisition of the NOESY. The ^1H-^{13}C-gHSQC spectrum was collected using a spectral win- dow of 8.5 and 31.5 kHz for ^1H and ^{13}C, respectively, and sampling each of the 512 increment with 64 scans.

Structure Calculations

The 3D structure of **L** in the 1:1 complex was obtained using a simulated annealing protocol through the Dynamo software [Dynamo]. On the basis of the relative intensity of the cross peaks in the NOESY spectra, NOEs have been classified as strong, medium, and weak, and an upper limit of 2.7, 3.3, and 5.0 Å has been applied, respectively, to restraint the corresponding interproton distance. The temperature was increased to 4000 K in 1000 initialization steps, then kept constant

for 4000 steps, and finally slowly decreased to 0 K during the 20000 steps cooling stage. A total of 100 structures were calculated. Neither DMF nor the Pd ion were present during the calculations. Gromos-53a6 force field parameters[3] were obtained through the ProDrg server (http://davapc1.bioch.dundee.ac.uk/prodrg/). The aliphatic hydrogens were introduced in the model using the standard parameters of the Dynamo force-field and the mass of the united-atom CH_2 atom type accordingly modified to represent the carbon only.

DFT Calculations

Hybrid-DFT calculations were carried out in order to predict the geometrical features of the complex PdL^{2+} and understand the spectroscopic features of **L** and its Pd complex. A comparison of the total electronic energies of the possible isomers of the 1:1 complex, featuring the metal ion in the Pd**L**Cl_2 complex coordinated by two chlorides and either two S atoms, or one S and one N, shows that all isomers fall within 12 kcal mol^{-1}, the isomer featuring S,S coordination being the least stable. The optimised geometry of Pd**L**Cl_2 in agreement with NMR data, shows the metal ion in a *pseudo*-square planar coordination geometry (Figure 3 in the paper) achieved by the N atom of the macrocycle and one neighboring sulfur atom. No interaction with the N atoms of the pyridine ring or the benzofurazan pendant is possible due to geometry constraint (optimised Pd···N2 distance: 3.034, 3.279, 3.287, 3.279 Å in the gas phase (Table S2), DMF (Table S3), water (Table S4) and acetonitrile (Table S5), respectively).

In agreement with UV–Vis absorption spectroscopy measurements, the band at the lowest energy (3.106 eV) calculated for **L** in the gas phase at TD-DFT level (Table S6) involves a π–π* HOMO-LUMO singlet monoelectronic excitation localized on the two cycles of the benzofurazan moiety (π-phenyl → π*-oxa-1,5-diazole). The low-energy absorption is calculated for Pd**L**Cl_2 to fall at higher energy, being due to excitation to the S14 and S16 excited states (3.824 and 3.621 eV, respectively), in agreement with the bathochromic shift observed during the titration of **L** with K_2PdCl_4. Both transitions are mainly due to monoelectronic excitations from the filled orbitals 124 and 125, localized on benzofurazan and the pyridine cycles, respectively, to the antibonding π-in-nature LUMO (MO 132; Figure S7). Solvation, accounted for at IEF-PCM SCRF level (Tables S7 and S8), results in a shift of the absorption bands towards higher wavelengths (S13, 3.621 and 3.618 eV in MeCN; S14, 3.681 and 3.678 eV in DMF). Based on TD-DFT calculations, it is therefore conceivable that excitation of the ligand results in an internal conversion to S1 excited state, from

which radiative emission occurs. On the contrary, in the complex Pd**L**Cl_2, the presence of the heavy metal would favor an ISC process to triplet states, responsible for the quenching of the emission at 540 nm.

DFT Calculations: Experimental

Theoretical calculations were performed with the Gaussian 09 (Rev. A.02)[6] suite of programs at Density Functional Theory (DFT) and TD-DFT level. The mPW1PW hybrid functional[7] was used along with Schäfer, Horn, and Ahlrichs double-ζ plus polarization all-electron basis sets (BSs) for C, H, N, O, Cl and S,[8] and LANL2DZ[9] with Relativistic Effective Core Potentials (RECPs) basis sets (BSs) for Pd.[10] The nature of the minima of each optimized structure was verified by harmonic frequency calculations. Natural[11] and Mulliken[12] atomic charge distributions were calculated at the optimized geometries at the same level of theory, and electronic transition energies and oscillator strengths were calculated at the TD-DFT level. The electronic spectra were simulated by a convolution of Gaussian functions centered at the calculated excitation wavelengths. In order to determine the influence of the solvent on the spectroscopic properties of the complexes, calculations were also carried out in the presence of acetonitrile, water, and DMF, implicitly taken into account by means of the Polarizable Continuum Model (PCM) approach in its Integral Equation Formalism variant (IEF-PCM),[13] which describes the cavity of the solute within the reaction field (SCRF) through a set of overlapping spheres. The program Molden 5.0[14] and GaussView 5[15] were used to investigate the charge distributions and molecular orbital shapes. GaussSum 2.0[16] was used for analyzing TD-DFT data. All calculations were carried out on a E4 workstation equipped with four quad-core AMD Opteron processors and 16 Gb of RAM and running the 64 bit version of the Ubuntu 12.4 Linux operating system.

Figure S7. Drawing of the isosurfaces calculated for the MOs 124 (filled), 125 (filled), and 132 (LUMO) for Pd**L**Cl_2. Cut-off value 0.05e.

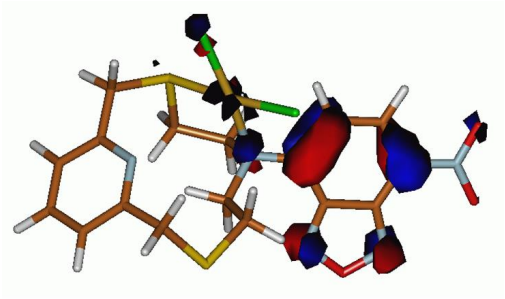

124

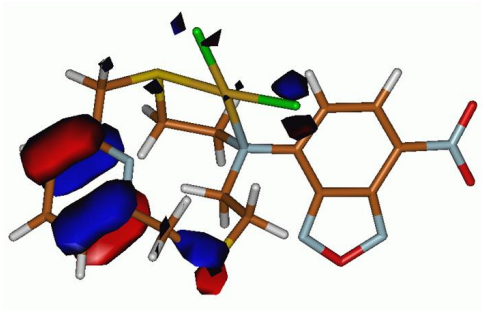

125

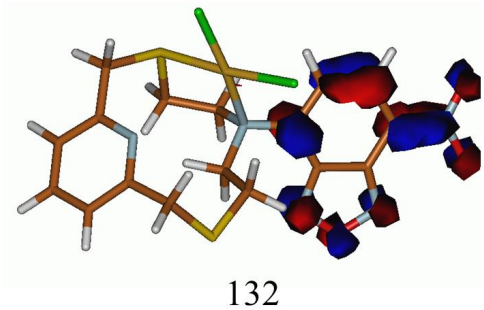

132

Table S2. Optimized geometry calculated for Pd**L**Cl_2 at DFT level in the gas phase in the orthogonal Cartesian coordinate format.

	x	y	z
C	-5.18072	2.30176	0.48793
C	-4.44285	2.51031	-0.66923
C	-3.44691	1.58399	-1.01180
N	-3.21079	0.51070	-0.25825
C	-3.92542	0.29285	0.84424
C	-4.92126	1.17556	1.26824
C	-3.67665	-0.99060	1.59160
S	-1.94477	-1.44602	1.92565
C	-1.18965	0.06337	2.61502
C	0.25805	0.11354	2.16784
N	0.43133	0.18698	0.68297
C	-0.13258	1.48124	0.18541
C	0.07503	1.72402	-1.30084
S	-1.15000	2.87781	-1.98260
C	-2.58672	1.76828	-2.23123
Pd	-0.89189	-1.44360	-0.14937
Cl	-2.33482	-3.16966	-0.66476
Cl	0.05357	-1.57964	-2.27748
C	1.84420	0.04267	0.40559
H	0.74950	0.98333	2.63600
H	0.78195	-0.79047	2.51004
H	-1.76385	0.94205	2.29385
H	-1.22830	0.01432	3.71239
H	0.03698	0.78059	-1.86770
H	1.05067	2.18908	-1.50289
H	-3.99051	-1.85173	0.97714
H	-4.21891	-1.01730	2.54583
H	-3.16296	2.24142	-3.03810
H	-2.22173	0.79486	-2.58611
H	0.27965	2.31438	0.77528
H	-1.20425	1.42035	0.38394
H	-4.62104	3.38204	-1.29991
H	-5.49079	0.97996	2.17781
H	-5.95762	3.00895	0.78373
C	2.78318	1.08414	0.72103
C	4.19419	0.93435	0.49305
C	4.67812	-0.29038	-0.05604
C	3.77548	-1.27472	-0.33160
C	2.37496	-1.11290	-0.09899
N	2.59311	2.27156	1.25926
N	4.79015	2.03814	0.89533
N	6.10154	-0.51120	-0.31898
H	4.14940	-2.20913	-0.74936
H	1.70331	-1.92654	-0.37230
O	6.42391	-1.59962	-0.73991
O	6.84565	0.41350	-0.09377
O	3.80703	2.81869	1.34830

Table S3. Optimized geometry calculated for Pd**L**Cl_2 at DFT level in DMF in the orthogonal Cartesian coordinate format.

	x	y	z
C	-0.141200	0.310070	-0.087760
C	-0.059030	0.322347	1.297680
C	1.187734	0.107660	1.902050
N	2.292393	-0.088820	1.181291
C	2.217449	-0.107820	-0.151470
C	1.014579	0.081862	-0.834030
C	3.496736	-0.318450	-0.910500
S	4.412667	-1.859590	-0.558130
C	3.140954	-3.165000	-0.518910
C	3.552655	-4.195670	0.508736
N	3.717342	-3.637520	1.899097
C	2.397987	-3.124800	2.385966
C	2.407200	-2.545750	3.791269
S	0.911497	-1.573300	4.133666
C	1.325372	0.050925	3.397619
Pd	5.006318	-1.858990	1.685349
Cl	6.297622	0.017520	1.183717
Cl	5.793617	-1.834370	3.907095
C	4.293498	-4.692710	2.704753
H	2.803428	-5.003470	0.532468
H	4.514109	-4.642780	0.226307
H	2.160264	-2.716610	-0.315800
H	3.098160	-3.637520	-1.509100
H	3.295474	-1.923060	3.967883
H	2.409855	-3.335220	4.555537
H	4.245678	0.444509	-0.650120
H	3.332797	-0.298220	-1.994990
H	0.622880	0.745678	3.877414
H	2.345314	0.325414	3.696057
H	1.643645	-3.919810	2.304743
H	2.126136	-2.331330	1.688427
H	-0.945420	0.487335	1.911031
H	0.984724	0.058389	-1.923630
H	-1.09706	0.471862	-0.588210
C	3.502723	-5.684940	3.380208
C	4.107615	-6.765200	4.113619
C	5.528291	-6.866970	4.158983
C	6.262365	-5.932640	3.487708
C	5.651193	-4.864070	2.771674
N	2.196673	-5.836390	3.467876
N	3.143288	-7.509120	4.612455
N	6.199992	-7.935050	4.885584
H	7.348333	-6.009760	3.511606
H	6.302707	-4.152000	2.267407
O	7.411946	-7.952470	4.870292
O	5.499314	-8.739010	5.459825
O	2.010451	-6.926230	4.208041

Table S4. Optimized geometry calculated for Pd**L**Cl_2 at DFT level in water in the orthogonal Cartesian coordinate format.

	x	y	z
C	-0.142150	0.299051	-0.091100
C	-0.063000	0.314469	1.294489
C	1.183575	0.107469	1.901859
N	2.290968	-0.084210	1.183986
C	2.218795	-0.106800	-0.148990
C	1.016335	0.075011	-0.834430
C	3.500383	-0.313990	-0.904910
S	4.415761	-1.856350	-0.555020
C	3.143284	-3.161100	-0.518640
C	3.552528	-4.193170	0.508358
N	3.718078	-3.636060	1.899434
C	2.399204	-3.122080	2.386351
C	2.408797	-2.540590	3.790612
S	0.910589	-1.572380	4.134339
C	1.318153	0.053126	3.397755
Pd	5.010220	-1.860580	1.687866
Cl	6.307265	0.014409	1.189607
Cl	5.796108	-1.840350	3.911305
C	4.293674	-4.692360	2.704132
H	2.801424	-4.999160	0.531647
H	4.512874	-4.642500	0.226009
H	2.162517	-2.712240	-0.317040
H	3.101876	-3.632320	-1.509490
H	3.295220	-1.914770	3.964863
H	2.415389	-3.328680	4.556254
H	4.248211	0.448730	-0.641100
H	3.339312	-0.291370	-1.989780
H	0.611000	0.744541	3.875530
H	2.335985	0.333224	3.698259
H	1.644698	-3.917030	2.306703
H	2.126846	-2.329980	1.687461
H	-0.951470	0.476134	1.905703
H	0.988822	0.048553	-1.924000
H	-1.097710	0.455016	-0.593930
C	3.502535	-5.680300	3.385538
C	4.107104	-6.76183	4.117405
C	5.527538	-6.86944	4.155205
C	6.261731	-5.93931	3.478162
C	5.651066	-4.86939	2.763925
N	2.196402	-5.82630	3.480948
N	3.142574	-7.50091	4.622956
N	6.198688	-7.93873	4.879984
H	7.347473	-6.02092	3.495765
H	6.303276	-4.16144	2.254664
O	7.410489	-7.96173	4.857871
O	5.498001	-8.73851	5.460263
O	2.009826	-6.91397	4.223986

Table S5. Optimized geometry calculated for Pd**L**Cl_2 at DFT level in acetonitrile in the orthogonal Cartesian coordinate format.

	x	y	z
C	-0.141200	0.310070	-0.087760
C	-0.059030	0.322347	1.297680
C	1.187734	0.107660	1.902050
N	2.292393	-0.088820	1.181291
C	2.217449	-0.107820	-0.151470
C	1.014579	0.081862	-0.834030
C	3.496736	-0.318450	-0.910500
S	4.412667	-1.859590	-0.558130
C	3.140954	-3.165000	-0.518910
C	3.552655	-4.195670	0.508736
N	3.717342	-3.637520	1.899097
C	2.397987	-3.124800	2.385966
C	2.407200	-2.545750	3.791269
S	0.911497	-1.573300	4.133666
C	1.325372	0.050925	3.397619
Pd	5.006318	-1.858990	1.685349
Cl	6.297622	0.017520	1.183717
Cl	5.793617	-1.834370	3.907095
C	4.293498	-4.692710	2.704753
H	2.803428	-5.003470	0.532468
H	4.514109	-4.642780	0.226307
H	2.160264	-2.716610	-0.315800
H	3.098160	-3.637520	-1.509100
H	3.295474	-1.923060	3.967883
H	2.409855	-3.335220	4.555537
H	4.245678	0.444509	-0.650120
H	3.332797	-0.298220	-1.994990
H	0.622880	0.745678	3.877414
H	2.345314	0.325414	3.696057
H	1.643645	-3.919810	2.304743
H	2.126136	-2.331330	1.688427
H	-0.945420	0.487335	1.911031
H	0.984724	0.058389	-1.92363
H	-1.097060	0.471862	-0.58821
C	3.502723	-5.684940	3.380208
C	4.107615	-6.765200	4.113619
C	5.528291	-6.866970	4.158983
C	6.262365	-5.932640	3.487708
C	5.651193	-4.864070	2.771674
N	2.196673	-5.836390	3.467876
N	3.143288	-7.509120	4.612455
N	6.199992	-7.935050	4.885584
H	7.348333	-6.009760	3.511606
H	6.302707	-4.152000	2.267407
O	7.411946	-7.952470	4.870292
O	5.499314	-8.739010	5.459825
O	2.010451	-6.926230	4.208041

Table S6. Monoelectronic excitation calculated for $PdLCl_2$ in the gas phase at IEF-PCM SCRF TD-DFT level. For each transition, the energy *E* (cm^{-1}), wavelength λ (nm), oscillator strength *f*, and the main contribution are listed. Only transitions with *f* > 0.05 are listed.

	E	λ	*f*	Major contributions
14	30846	324.2	0.0537	H-7->LUMO (25%), H-6->LUMO (63%)
16	31675	315.7	0.1311	H-7->LUMO (65%), H-6->LUMO (23%)
30	36197	276.3	0.0518	H-19->L+1 (10%), H-7->L+1 (12%), H-6->L+1 (43%)
48	40374	247.7	0.0697	H-19->L+1 (11%), H-9->L+1 (19%), H-5->L+4 (33%), H-4->L+4 (10%)
50	40614	246.2	0.0601	H-9->L+1 (10%), H-5->L+4 (56%)
59	43077	232.1	0.0881	H-19->LUMO (14%), H-6->L+3 (10%), H-2->L+5 (32%)
60	43278	231.1	0.0896	H-13->L+1 (16%), H-10->L+1 (18%), H-6->L+3 (15%), H-2->L+5 (11%), H-1->L+5 (17%)
63	44385	225.3	0.0595	H-14->L+1 (63%)
85	48639	205.6	0.0861	H-9->L+3 (28%), H-6->L+4 (44%)
117	54392	183.9	0.0759	H-14->L+4 (13%), H-4->L+8 (10%), HOMO->L+9 (17%)
118	54624	183.1	0.0808	H-4->L+8 (24%), HOMO->L+9 (23%)
119	54640	183.0	0.0502	H-7->L+5 (25%)
128	55162	181.3	0.0636	H-13->L+4 (18%), H-1->L+9 (40%)
129	55554	180.0	0.0546	H-18->L+2 (11%), H-9->L+5 (46%)
134	56187	178.0	0.0588	H-19->L+3 (26%), H-18->L+3 (12%), H-17->L+3 (11%), H-15->L+3 (12%)
135	56405	177.3	0.0963	H-15->L+2 (22%), H-11->L+5 (27%)
148	57354	174.4	0.0521	
193	61401	162.9	0.0533	H-22->L+3 (16%), H-21->L+3 (16%), H-1->L+13 (16%)
194	61421	162.8	0.0698	H-22->L+3 (17%), H-21->L+3 (18%), H-1->L+13 (19%)
199	61788	161.8	0.0730	H-24->L+2 (11%), H-23->L+2 (51%)

Table S7. Monoelectronic excitation calculated for Pd**L**Cl_2 in MeCN at IEF-PCM SCRF TD-DFT level. For each transition, the energy E (cm^{-1}), wavelength λ (nm), oscillator strength f, and the main contribution are listed. Only transitions with $f > 0.05$ are listed.

	E	λ	*f*	Major contributions
13	29205	342.4	0.0917	H-7->LUMO (24%), H-6->LUMO (70%)
14	29688	336.8	0.1728	H-7->LUMO (67%), H-6->LUMO (25%)
31	37606	265.9	0.0568	H-13->LUMO (27%), H-12->LUMO (12%), H-9->L+1 (30%)
34	38420	260.3	0.0701	H-9->L+1 (22%), H-3->L+2 (12%)
35	38688	258.5	0.0531	H-20->LUMO (11%), H-15->LUMO (34%), H-14->LUMO (15%)
51	43228	231.3	0.0711	H-20->LUMO (13%), H-12->L+1 (18%), H-12->L+2 (21%)
52	43426	230.3	0.0999	H-13->L+1 (28%), H-12->L+2 (16%)
76	48603	205.7	0.0926	H-7->L+3 (22%), H-6->L+4 (49%)
105	53531	186.8	0.0597	H-9->L+4 (10%), H-4->L+7 (42%), H-3->L+7 (16%)
106	53642	186.4	0.0536	H-2->L+8 (22%), HOMO->L+8 (45%)
108	54019	185.1	0.1122	H-7->L+5 (35%)
109	54108	184.8	0.1614	H-10->L+4 (12%)
110	54256	184.3	0.0793	H-28->LUMO (20%), H-26->LUMO (10%)
112	54619	183.1	0.0503	H-28->LUMO (19%), H-2->L+8 (10%), H-1->L+8 (36%)
119	55486	180.2	0.118	H-24->L+1 (15%), H-11->L+3 (11%)
120	55515	180.1	0.1138	H-24->L+1 (16%), H-4->L+8 (11%), H-2->L+8 (16%)
124	56087	178.3	0.0817	H-15->L+3 (14%), H-14->L+3 (30%)
125	56129	178.2	0.0698	H-29->LUMO (10%), H-14->L+3 (12%), H-4->L+8 (14%), H-3->L+8 (21%)
127	56430	177.2	0.0584	H-11->L+4 (55%)
132	57061	175.3	0.0576	H-18->L+2 (49%)
134	57205	174.8	0.1163	H-5->L+8 (36%)
140	57896	172.7	0.0724	H-32->LUMO (19%), H-31->LUMO (16%), H-18->L+2 (10%), H-9->L+5 (14%)
150	58732	170.3	0.0762	H-6->L+7 (24%), H-1->L+9 (32%)
172	61213	163.4	0.0544	H-2->L+11 (44%)
182	61951	161.4	0.0706	H-15->L+5 (11%), H-9->L+6 (20%)
193	62742	159.4	0.0651	H-15->L+5 (14%), H-3->L+11 (21%)

Table S8. Monoelectronic excitation calculated for Pd**L**Cl_2 in DMF at IEF-PCM SCRF TD-DFT level. For each transition, the energy E (cm^{-1}), wavelength λ (nm), oscillator strength f, and the main contribution are listed. Only transitions with $f > 0.05$ are listed.

	E	λ	*f*	Major contribs
13	29181	342.7	0.1080	H-7->LUMO (29%), H-6->LUMO (65%)
14	29656	337.2	0.1663	H-7->LUMO (63%), H-6->LUMO (29%)
31	37590	266.0	0.0619	H-13->LUMO (26%), H-12->LUMO (12%), H-9->L+1 (32%)
34	38400	260.4	0.0685	H-9->L+1 (21%), H-3->L+2 (14%)
35	38670	258.6	0.0555	H-20->LUMO (11%), H-15->LUMO (35%), H-14->LUMO (15%)
51	43213	231.4	0.0934	H-20->LUMO (11%), H-12->L+1 (20%), H-12->L+2 (18%)
52	43408	230.4	0.0884	H-13->L+1 (26%), H-12->L+2 (19%)
76	48578	205.9	0.0953	H-7->L+3 (23%), H-6->L+4 (51%)
105	53527	186.8	0.0756	H-9->L+4 (10%), H-4->L+7 (42%), H-3->L+7 (16%)
106	53627	186.5	0.0535	H-2->L+8 (23%), HOMO->L+8 (45%)
108	53985	185.2	0.1155	H-10->L+4 (11%), H-7->L+5 (31%)
109	54076	184.9	0.1882	H-10->L+3 (10%), H-10->L+4 (11%), H-4->L+7 (10%)
110	54239	184.4	0.0598	H-28->LUMO (20%), H-26->LUMO (11%), H-1->L+8 (10%)
115	55014	181.8	0.0548	H-14->L+3 (22%), H-13->L+3 (21%), H-12->L+3 (11%), H-10->L+4 (11%), H-8->L+5 (12%)
118	55356	180.6	0.0569	H-11->L+3 (13%), H-3->L+7 (15%)
119	55466	180.3	0.1672	H-11->L+3 (11%)
124	56080	178.3	0.0718	H-15->L+3 (14%), H-14->L+3 (28%), H-5->L+6 (11%)
125	56108	178.2	0.0694	H-14->L+3 (12%), H-4->L+8 (16%), H-3->L+8 (25%)
127	56419	177.2	0.0617	H-11->L+4 (54%)
132	57016	175.4	0.0630	H-18->L+2 (50%)
134	57189	174.9	0.1154	H-5->L+8 (37%)
140	57864	172.8	0.0739	H-32->LUMO (19%), H-31->LUMO (17%), H-9->L+5 (14%)
150	58722	170.3	0.0754	H-6->L+7 (26%), H-1->L+9 (30%)
170	61063	163.8	0.0526	H-13->L+4 (11%), H-13->L+5 (20%), H-12->L+4 (15%), H-11->L+5 (10%), H-10->L+5 (13%)

172	61204	163.4	0.0526H-2->L+11 (43%)
182	61946	161.4	0.0711H-17->L+3 (11%), H-15->L+5 (11%), H-9->L+6 (19%)
193	62739	159.4	0.0629H-15->L+5 (13%), H-3->L+11 (20%)

Photophysical measurements

Absorption spectra were recorded on a Perkin-Elmer Lambda 45. For the fluorescence spectroscopy measurements, uncorrected emission and corrected excitation spectra were obtained with a Perkin-Elmer LS 55 spectrofluorimeter. Luminescence quantum yields (uncertainty ± 15%) were determined using fluorescein in NaOH 0.1 M (Φ = 0.92) as a reference. In order to allow comparison of emission intensities, corrections were performed for instrumental response, inner filter effects, and phototube sensitivity[17]. Values of $\log K_a$ were obtained by fitting spectrophotometric and spectrofluorimetric data with SPECFIT/32®, a global analysis software.

The determination of the nanoparticles hydrodynamic diameter distributions was carried out through Dynamic Light Scattering measurements employing a Malvern Nano ZS instrument equipped with a 633 nm laser diode. A Philips CM 100 transmission electron microscope operating at 80 kV was used for TEM investigations.

Figure S8. A) TEM images and B) size distribution (d=10 ± 1 nm) of **DEAC@NPs,** C) a schematic representation of the **NP** and D) Dynamic Light Scattering (DLS) measurement of **NPs**; D_H=24nm, PDI=0.10 (PdI=$(\sigma/Zavg)^2$).

.

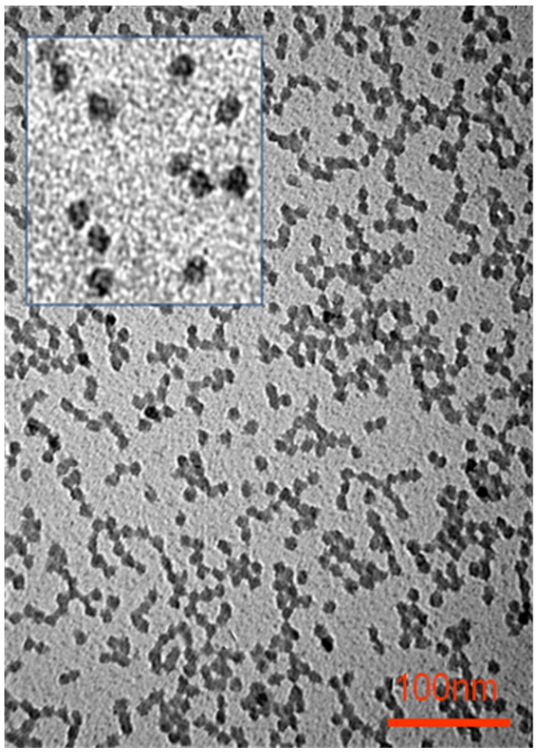

(A)

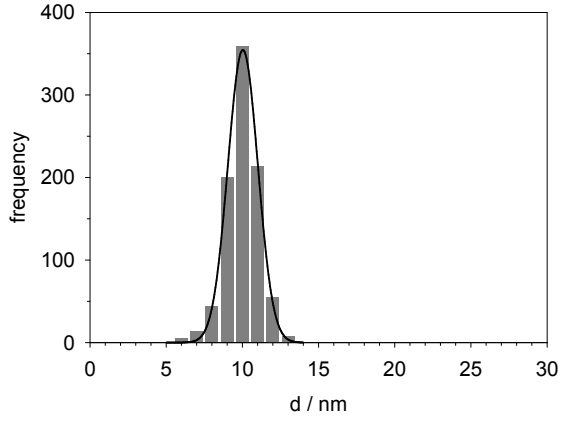

(B)

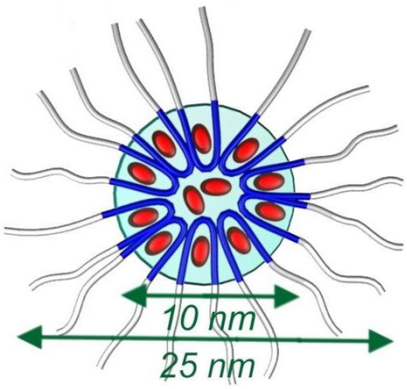

(C)

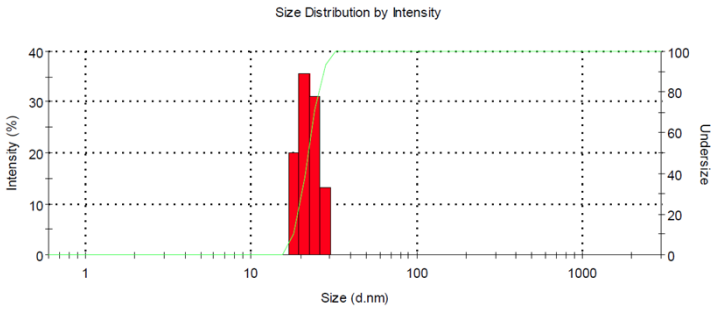

(D)

Figure S9. Absorption spectra of **DEAC@NPs** $1.25 \cdot 10^{-7}$ M in water by adding increasing amounts of **L** ($4.76 \cdot 10^{-4}$ M in AN), and absorbance trends at 423 and 504 nm.

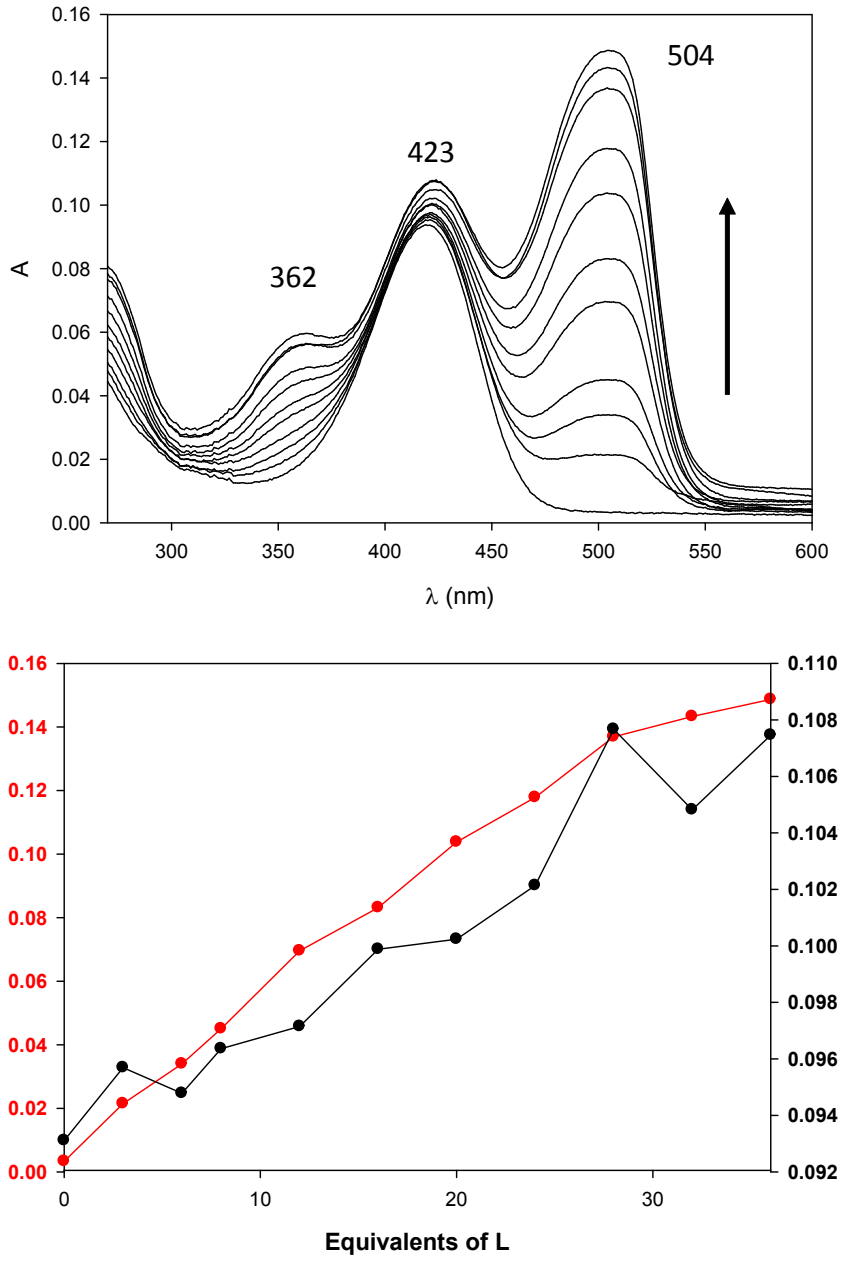

Figure S10. Emission spectra of 1.25×10^{-7} M **DEAC@NP**s in water (λ_{ex}=400 nm) and trends of emission intensity at 464 nm (●) and 528 nm (○) upon addition of increasing amounts of **L** 4.76×10^{-4} M in AN.

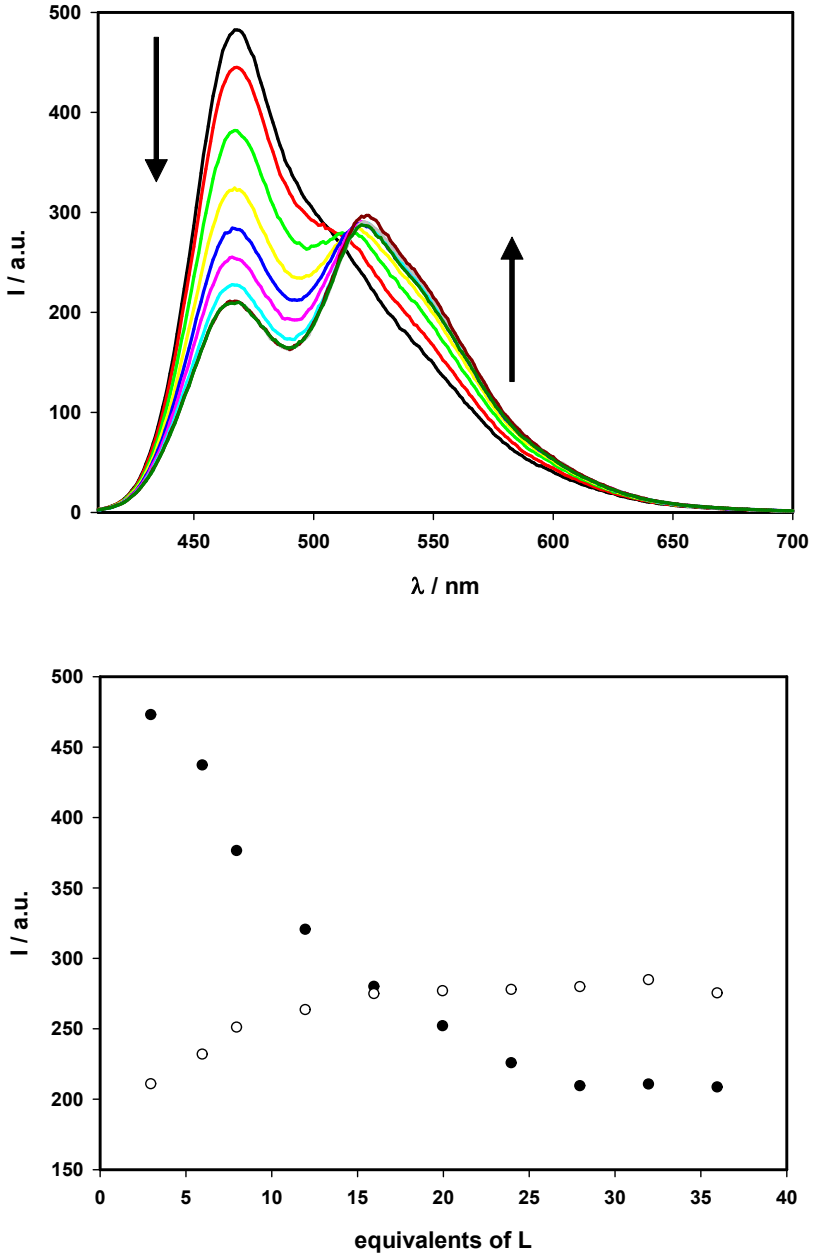

Calculation of the average number of L per nanoparticles

We refer to Figure S8 in order to calculate the number of **L** per nanoparticles and report here the spectrum with the highest absorbance (Figure S13).

Figure S11. Absorption spectrum of DEAC-doped NPs $1.25 \cdot 10^{-7}$ in water after the addition of 36 equivalents of **L** $4.76 \cdot 10^{-4}$ M in MeCN.

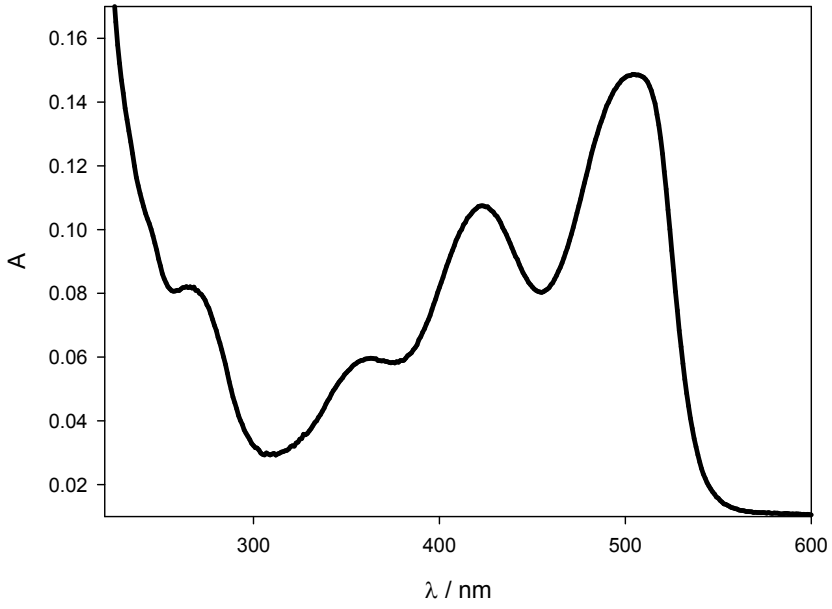

The absorbance at 504 nm is equal to 0.1487. As mentioned in the text, we assume the molar absorption coefficient of **L** to be 3.3×10^4 $M^{-1}cm^{-1}$. Applying the Beer-Lambert law we obtain the concentration of **L**:

$$c = \frac{A}{\varepsilon d} = \frac{0.1487}{3.3x10^4 \cdot 1} = 4.51x10^{-6}\, M$$

Dividing *c* by the concentration of NPs (1.25×10^{-7} M) we obtain the number of fluorophores per nanoparticle, that is equal to 36.

Figure S12. Relative emission intensity at 528 nm of **L:**DEAC@NPs 20:1 with **L** and K_2PdCl_4 in 1:1 molar ratio and in the co-presence of 10 equivalents of Hg^{II}, Cd^{II}, Pb^{II}, Zn^{II}, Co^{II}, Ni^{II}, Ag^{I}, Cu^{II} as nitrate or perchlorate salts and K_2PtCl_4. Measurements were made soon after the mixing of the reactants and were stable in time.

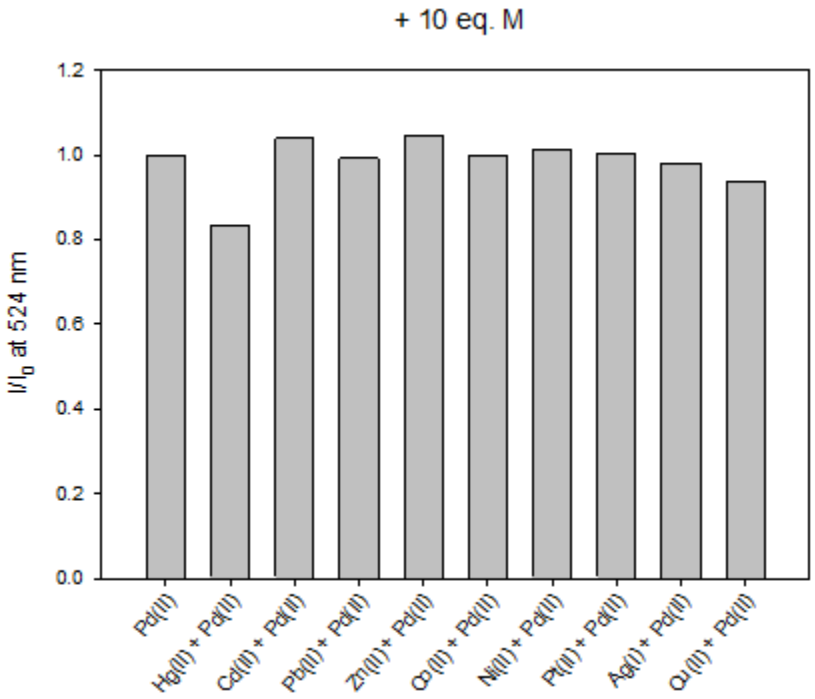

Figure S13. Absorption (left) and emission spectra (right, λ_{ex}= 450 nm) **L**@NPs 1:3 ([**L**]= $1.0 \cdot 10^{-6}$ M, [NPs]= $3 \cdot 10^{-6}$ M) with K_2PdCl_4 $4.0 \cdot 10^{-4}$ M at 298 K ([K_2PdCl_4] = 0 → 1.1×10^{-6} M).

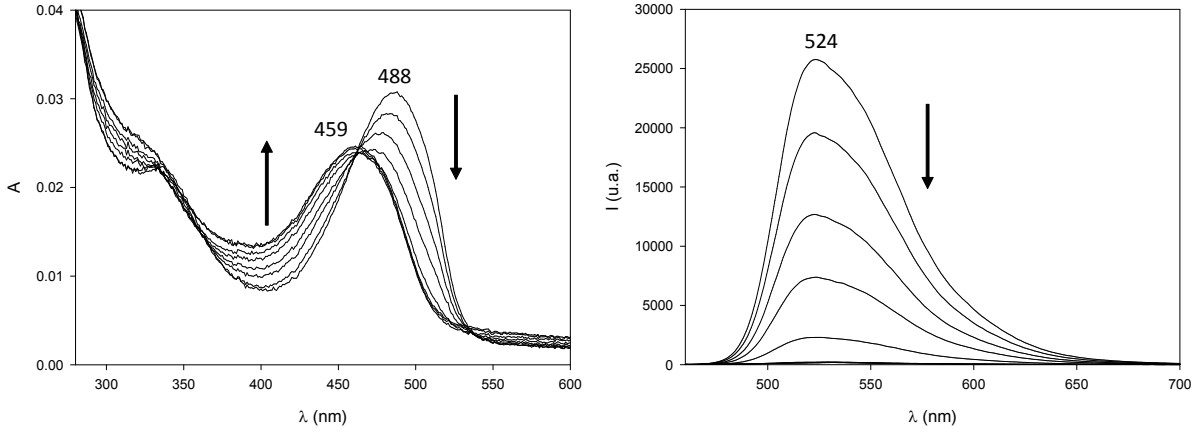

Figure S14. Job plot for the coordination of Pd^{II} with **L**@NPs 20:1.

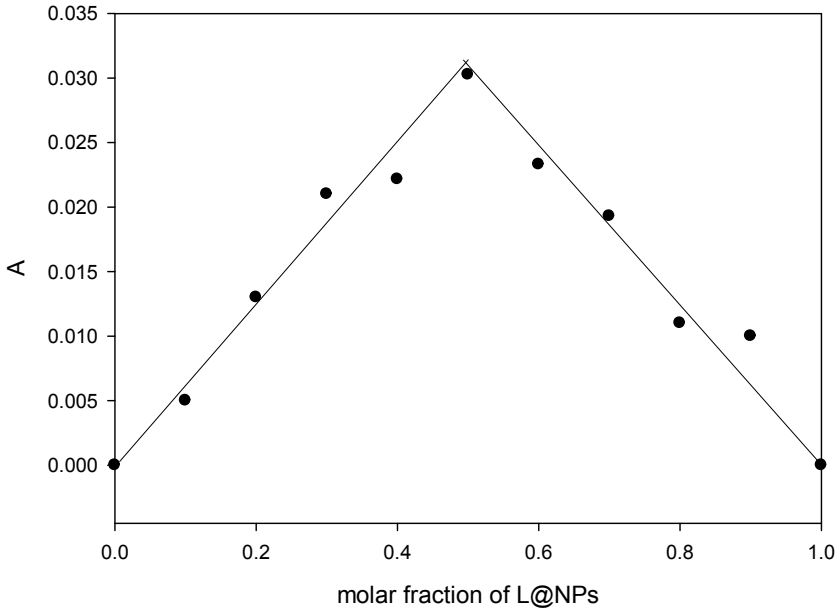

References

[1] A.J. Blake, A. Bencini, C. Caltagirone, G. De Filippo, L.S. Dolci, A. Garau, F. Isaia, V. Lippolis, P. Mariani, L. Prodi, M. Montalti, N. Zaccheroni, C. Wilson, *Dalton Trans*, 2004, 2771.

[2] J. Cavanagh, W. J. Fairbrother, A. G. Palmer III, M. Rance, N. J. Skelton, *Protein NMR Spectroscopy - Principles and Practice*; 2nd ed.; Elsevier Academic Press: Oxford, U.K., 2007.

[3] Dynamo: *the NMR molecular dynamics and analysis system* http://spin.niddk.nih.gov/NMRPipe/dynamo.

[4] C. Oostenbrink, A. Villa, A.W. F. Van Gunsteren, *J Comput Chem*, 2004, **25**, 1656.

[5] T. Yamaji, T. Saito, K. Hayamizu, O. Yamamoto, M. Yanagisawa, N. Wasada, K. Someno, S. Kinugasa, K. Tanabe, J. Hiraishi, *J. SDBSWeb* (National Institute of Advanced Industrial Science and Technology) http://riodb01.ibase.aist.go.jp/sdbs/ (accessed Sep, 2013).

[6] Gaussian 09, Revision A.02, M. J. Frisch, G. W. Trucks, H. B. Schlegel, G. E. Scuseria, M. A. Robb, J. R. Cheeseman, G. Scalmani, V. Barone, B. Mennucci, G. A. Petersson, H. Nakatsuji, M. Caricato, X. Li, H. P. Hratchian, A. F. Izmaylov, J. Bloino, G. Zheng, J. L. Sonnenberg, M. Hada, M. Ehara, K. Toyota, R. Fukuda, J. Hasegawa, M. Ishida, T. Nakajima, Y. Honda, O. Kitao, H. Nakai, T. Vreven, Jr. J. A. Montgomery, J. E. Peralta, F. Ogliaro, M. Bearpark, J. J. Heyd, E. Brothers, K. N. Kudin, V. N. Staroverov, R. Kobayashi, J. Normand, K. Raghavachari, A. Rendell, J. C. Burant, S. S. Iyengar, J. Tomasi, M. Cossi, N. Rega, J. M. Millam, M. Klene, J. E. Knox, J. B. Cross, V. Bakken, C. Adamo, J. Jaramillo, R. Gomperts, R. E. Stratmann, O. Yazyev, A. J. Austin, R. Cammi, C. Pomelli, J. W. Ochterski, R. L. Martin, K. Morokuma, V. G. Zakrzewski, G. A. Voth, P. Salvador, J. J. Dannenberg, S. Dapprich, A. D. Daniels, Ö. Farkas, J. B. Foresman, J. V. Ortiz, J. Cioslowski, D. J. Fox, Gaussian, Inc., Wallingford CT, 2009.

[7] C. Adamo, V. Barone, *J. Chem. Phys.*, 1998, **108**, 664–675.

[8] A. Schäfer, H. Horn, R. Ahlrichs, *J Chem Phys*, 1992, **97**, 2571.

[9] T. H. Jr. Dunning, P. J. Hay in *"Methods of Electronic Structure, Theory"*, Vol. 2, H. F. Schaefer III ed., Plenum Press, 1977; J. V. Ortiz, P. J. Hay, R. L. Martin, *J Am Chem Soc*, 1992, **114**, 2736.

[10] Basis sets were obtained from Basis Set Exchange and Basis Set EMSL Library. D. Feller, J. *Comp Chem*, 1996, **17**, 1571; K. L. Schuchardt, B. T. Didier, T. Elsethagen, L. Sun, V. Gurumoorthi, J. Chase, J. Li, T. L. Windus, *J Chem Inf Model*, 2007, **47**, 1045.

[11] A. E. Reed, R. B. Weinstock, F. Weinhold, *J Chem Phys*, 1985, **83**, 735.

[12] R. S. Mulliken, J. Chem. Phys., 1955, **23**, 1833.

[13] J. Tomasi, B. Mennucci, R. Cammi, *Chem Rev*, 2005, **105**, 2999.

[14] G. Schaftenaar, J. H. Noordik, *J Comput -Aided Mol Des*, 2000, **14**, 123.

[15] R. Pennington, T. Keith, J. Millam, GaussView, Version 5, Semichem Inc., Shawnee Mission KS, 2009.

[16] N. M. O'Boyle, A. L. Tenderholt, K. M. Langner, J. Comp. Chem., 2008, **29**, 839.

[17] A. Credi, L. Prodi, Inner filter effects and other traps in quantitative spectrofluorimetric measurements: Origins and methods of correction, J Mol Struct, DOI: 10.1016/j.molstruc.2014.03.028